http://ansinet.com/itj

ITJ

ISSN 1812-5638

INFORMATION TECHNOLOGY JOURNAL

ANSInet
Asian Network for Scientific Information
308 Lasani Town, Sargodha Road, Faisalabad - Pakistan

Information Technology Journal 12 (22): 6925-6932, 2013
ISSN 1812-5638 / DOI: 10.3923/itj.2013.6925.6932

Structural Design and Analysis of Megawatt Wind Power Gear Boxes

Lu Dong, Li Hou, Zhi-jun Sun and Wei Xu
School of Manufacturing Science and Engineering, Sichuan University, Chengdu, 610065, China

Abstract: In this study, for the problems of detection difficulty and high mechanical performance requirement of megawatt wind power gear boxes, the gear box structure is designed and the finite element models of the box body and the gear box are established. First, force calculation and static analysis were performed when the box body undertaked 1.4 times of the rated load. The box body structure was improved under the condition of meeting rigidity and strength requirements: the materials of the upper and lower box bodies which bear less force were composed of QT350 instead of QT400, so as to save costs. Furthermore, the gearbox was supported by elasticity rather than fixation. Modal analyses were, respectively performed and the comparison showed that supported by elasticity could reduce vibration more effectively. Finally, the system's frequency catching was analyzed on this basis. The results show that the system has no frequency catching, thus it cannot produce resonance and the structure is safe. The research has been applied to relevant equipments and is shown to run well, thereby providing a reference for actual manufacture.

Key words: Gear box, statics analysis, modal analysis, structural improvement, frequency catching

INTRODUCTION

Gear boxes, as an important component in wind turbine generators, are mainly used for transferring the power produced by wind wheels in wind to the generator and adjusting the generator's speed to the required speed. The box body is the key component of the gear box and undertakes the acting force of the wind wheels and all loads produced by the gear in transmission, thus the box body must be sufficiently strong and rigid to ensure the transmission quality. The gear box must undertake wind action produced by irregular turning and variable load, as well as the impact of strong wind, thus it is very difficult to repair once it is failed. Therefore, research regarding the dynamic performance of the gear box has important significance.

The rigidity and the intensity of the gear box have been researched thoroughly throughout the world and many optimization programs (Yi *et al*., 2012; Kusiak and Li, 2011; Tian *et al*., 2011) have been established for them. At present, the most common method adopted both in China and elsewhere for researching the dynamic characteristics of the gear box is to first utilize the modal analysis method to determine the inherent frequency and mode of the vibration of the system in each stage, then adopt the vibration superposition method to perform dynamic response analysis, thereby determining the system's dynamic response under all vibration resources (Ge *et al*., 2010; Herbert *et al*., 2010; Soua *et al*., 2011). An important objective of dynamic performance analysis is to avoid resonance, as frequency catching analysis can describe the catching characteristics of the system when its excitation frequency draws close to its inherent frequency, thereby laying the foundation for reducing vibration and avoiding resonance for the system (Zhang *et al*., 2009; Han *et al*., 2008). However, throughout the world there have been few research reports concerning the frequency catching characteristics of large gear boxes in operation.

Due to the complexity of the structure of the wind power gear box, the traditional method cannot meet the design requirements, therefore this study adopts the finite element method to emphasize the analysis of the static characteristics of the box body of the gear box under 1.4 times of rated load and the overall inherent characteristics of the gear box and uses Matlab software to analyze the frequency catching of the gear box.

STRUCTURAL STYLE OF WIND POWER GEAR BOX

The configuration of the drive shaft and gear of the 2.0 MW wind power gear box used in this study are shown in Fig. 1.

As shown in Fig. 1, the gear box adopts one-stage planet transmission and two-stage fixed-axis transmission and shafts I, II and III are three drive shafts of the ordinary gear train, among which shaft III is a low-speed

Corresponding Author: Li Hou, School of Manufacturing Science and Engineering, Sichuan University, Sichuan, Chengdu, 610065, China

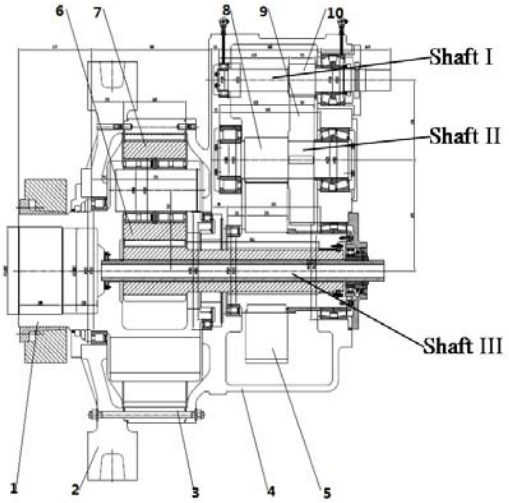

Fig. 1: Structural drawing of gear box assembly, 1. planet carrier, 2: Torque arm, 3: Inner gear ring, 4: Upper and lower box bodies of ordinary gear train, 5: Level-II big gear, 6: Center wheel, 7: Planet wheel, 8: Level-II small gear, 9: Level-III big gear, 10: Level-III small gear

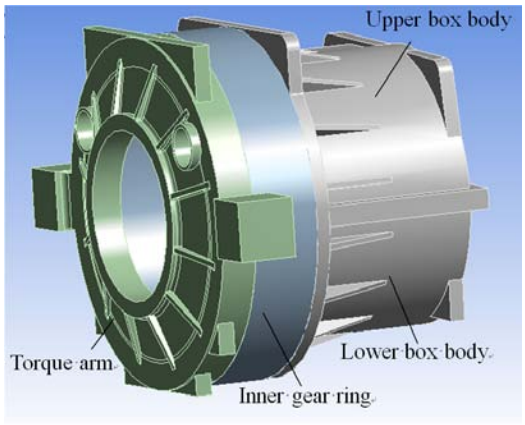

Fig. 2: Model of box body

input shaft and shaft I is a high-speed output shaft. These are arranged in a triangular design so that the gear box has more compact structure, smaller volume and lower cost and the center of the gear box is more concentrated, thereby strengthening stability.

The main technical parameters of the gear box are shown in Table 1.

After omitting the local smaller structures with smaller amounts of influence, such as the lifting ring, boss, oil groove, casting of curves, assembly of transitional surface, etc., the geometric model of the box body of the gear box which was established using Solidworks software, is shown in Fig. 2. It is mainly composed of the upper and lower box bodies of the ordinary gear train, the torque arm and the inner gear ring of the planetary gear train. Fig. 3 shows the overall diagrammatic figure of the gear box.

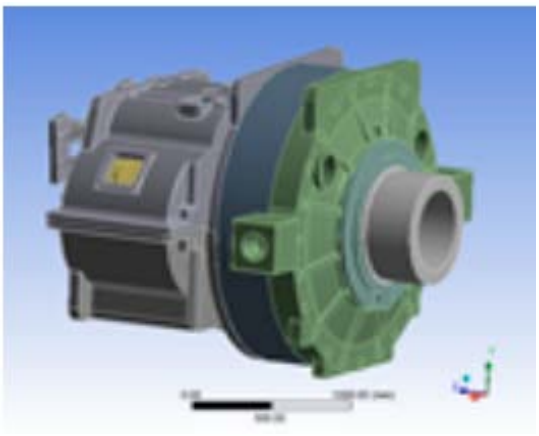

Fig. 3: Model of whole gearbox

Table 1: Technical parameters of the gearbox

Type	Value	Type	Value
Rated Power	2250 KW	Safety factor for ultimate load	3
Rated input speed	15.17 r m^{-1}	Lubrication method	Oiled injection
Rated output speed	1800 r m^{-1}	Weight	20T
Speed increasing ratio	118.6		

STATIC LOAD CALCULATION OF BOX BODY

To analyze the static strength of the box body of the gear box, the forcing of each part of the box body must be calculated first.

Load calculation of planetary gear train: The transmission structure drawing of the gear box is shown in Fig. 4, in which the numbers of the gears and key components in this figure correspond to Fig. 1 and H is the planet carrier.

All gears in the gear box are helical gears, so that power loss in the transmission can be neglected, leaving the following (Yao and Song, 2009):

$$T_7 = 9550\frac{P}{n}\cdot K_A = 9550\times\frac{2250}{15.17}\times 1.4 = 1.98\times 10^6\ N\cdot m \quad (1)$$

Where:

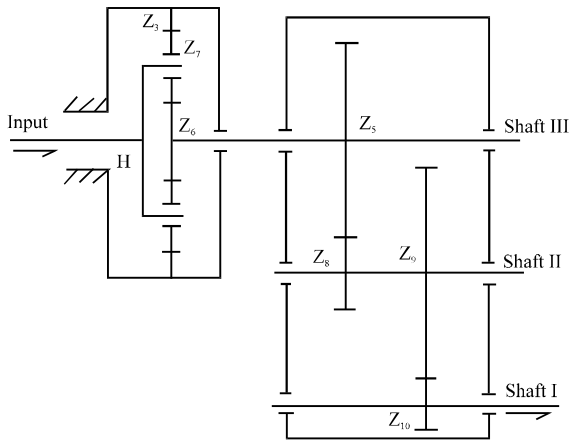

Fig. 4: Transmission structure of the gearbox, H: Planet carrier; 3. Inner gear ring; 5: Level-II big gear; 6. center wheel, 7: Planet wheel, 8: Evel-II small gear, 9: Level-III big gear, 10: Level-III small gear

T7 = Input torque of the planet carrier
P = Power of generator, P = 2250KW
n = Input speed, n = 1517 rm
K_A = Service factor without load spectrum; and K_A is 1.4

$$i_{63}^{H}=\frac{n_6-n_H}{n_3-n_H}=-\frac{z_6}{z_3}=-5 \quad (2)$$

Where:
i^{H}_{63} = Transmission ratio of planet gear train;
n_3, n_6, z_3, z_6 = Speed and number of teeth of components 3 and 6; and
n_H = Speed of the planet carrier

The inner gear ring is stationary, i.e., $n_3 = 0$, so $n_6 = 6n_H$. Therefore, the torque distribution relation of the differential gear train is shown as follows:

$$\frac{T_6}{T_H}=-\frac{1}{i_{6H}^{3}},\ \frac{T_6}{T_3}=-\frac{1}{i_{63}^{H}} \quad (3)$$

The torque distributed on the center wheel and the inner gear ring is shown as follows:

$$\begin{cases} T_6=-\dfrac{1}{i_{6H}^{3}}T_H=-\dfrac{n_H}{n_6}T_H=-\dfrac{1}{6}T_H \\ T_3=-i_{63}^{H}T_H=-5T_H \end{cases} \quad (4)$$

T_3 and T_6 can be calculated according to equation 1.

Load calculation of ordinary gear train: Shaft III is the output shaft of the ordinary gear train and is also the input shaft of the planetary gear train, so that $T_c = T_6$, where T_c represents the torque on shaft III.

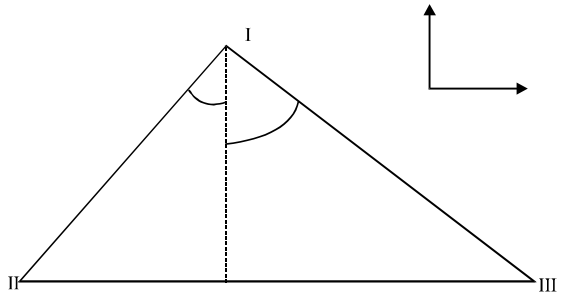

Fig. 5: Positional relationship of the ordinary gear train'sdrive shafts

However:

$$\frac{T_c}{T_b}=-i_{85}=-\frac{z_5}{z_8}=-\frac{88}{19}$$

in which the torque on shaft II is:

$$T_b=-\frac{19}{88}T_c$$

and

$$\frac{T_b}{T_a}=-i_{109}=-\frac{z_9}{z_{10}}=-\frac{111}{26}$$

in which the torque on shaft I is:

$$T_a=-\frac{26}{111}T_b$$

The three shafts of the ordinary gear train are arranged in a triangular formation and their positions are shown in Fig. 5. It is regulated that shaft Z is the axial direction, the positive direction of the radial shaft X faces rightwards horizontally, the positive direction of radial shaft Y faces straight up and axial force can be directly applied on the retainer ring on the outer ring of the bearing. All radial forces should be projected to shafts X and Y and must then be further loaded to the bearing holes for installation.

A, B and C in this figure represent the center distances of the three shafts; it is known that A = 650 mm, B = 690 mm, C = 496 mm and their triangular relationship is shown as follows:

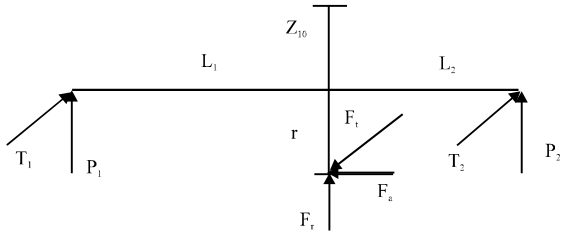

Fig. 6: Map of shaft 2's stress

$$\begin{cases} \frac{1}{2}H \cdot B = \sqrt{P(P-A)(P-B)(P-C)} \\ P = \frac{A+B+C}{2} \\ \cos\alpha = \frac{H}{A} \\ \cos\gamma = \frac{H}{C} \end{cases}$$

It can be obtained that H = 446 mm, $\alpha = 46.7^{\circ}$ and $\gamma = 25.9^{\circ}$.

Force is analyzed by taking shaft I as an example and shaft I mainly undertakes the support force (T_1, P_1, T_2, P_2) of the front and the rear bearing seats and the normal force of gear 10, as shown in Fig. 6.

According to the force analysis method of the helical gear, the normal force can be decomposed to three orthogonal forces, namely F_t, F_r, F_a in the following figure (Yao and Song, 2009):

$$\begin{cases} F_t = \frac{2T_a}{d} \\ F_r = \frac{F_t \tan\alpha_n}{\cos\beta} \\ F_a = F_t \tan\beta \end{cases} \quad (5)$$

where α_n and β are respectively normal pressure angle and helical gear thread angle which are known. The values of F_t, F_r and F_a can be calculated through T_a and the following formula can be determined through Fig. 6.

$$\begin{cases} F_r + P_1 + P_2 = 0 \\ T_1 + T_2 = F_t \\ F_a \cdot r_{10} + P_1 \cdot L_1 = P_2 \cdot L_2 \\ T_1 \cdot L_1 = T_2 \cdot L_2 \end{cases} \quad (6)$$

The values of T_1, P_1, T_2 and P_2 can be calculated through equation 6. They are, respectively projected to shafts X and Y, by taking T_1 and P_1 as examples and their orthogonal decomposition is shown in Fig. 7.

The component forces of T_1 and P_1 in the X and Y directions can be determined through Fig. 7:

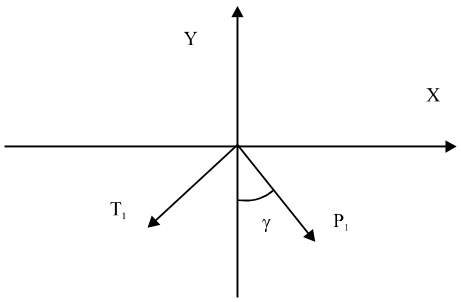

Fig. 7: The orthogonal decomposition of shaft 2's stress

$$\begin{cases} F_x = P_1 \cdot \sin\gamma - T_1 \cdot \cos\gamma \\ F_y = -(P_1 \cdot \cos\gamma + T_1 \cdot \sin\gamma) \end{cases} \quad (7)$$

F_x and F_y are the forces of shaft I in the front bearing hole; similarly, the component forces of T_2 and P_2 in the X and Y directions can be determined, namely the force of shaft I at the rear bearing hole. The forces of shafts II and III can be calculated using the same method and the loads obtained are shown in Table 2.

ANALYSIS AND STRUCTURAL IMPROVEMENT OF BOX BODY

In the preliminary design, the inner gear ring of the box body is composed of 17CrNi2Mo and other parts are composed of QT400. According to the diagrammatic Fig. 2 of the box body while considering the dead weight of the box body, the gravity is loaded on the gravity center, the reaction force of the bearing is transformed to loads in directions X, Y and Z according to Table 2 and the loads are loaded on the corresponding bearing hole. Then the Ansys software is adopted to perform further static analysis for the box body, thereby obtaining the displacement and stress nephogram of the box body under 1.4 times of rated load, as shown in Fig. 8.

As shown in Fig. 8, the maximum displacement of the box body is 3.9398 mm and it is located on the upper box body, therefore the rigidity meets the design requirements. The maximum stress is 245.28 MPa and it is loaded on the left support of the torque arm. Since the limit of yielding of the QT400 is 250 MPa, the more dangerous torque arm is also safe.

Through analysis it is found that the stress of the box body is mainly distributed throughout the torque arm and the stress values of the other components are smaller, therefore the structure is improved: the relatively safe upper and lower box bodies are composed of QT350 rather than Qt 400, their limits of yielding are both 220 MPa and QT350 can still ensure that the box body has ample

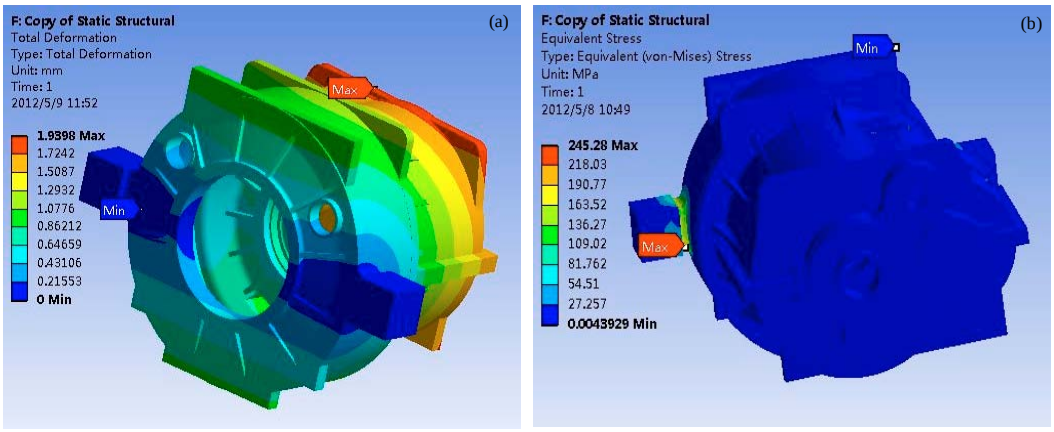

Fig. 8(a-b): Displacement and stress of the box body, (a) The displacement nephogram (b) The stress nephogram

Table 2: Loads in bearing holes of the gearbox

	Force/N	X	Y	Z
I	Front bearing hole	-3.30×10^{4}	-4.24×10^{4}	-4.14×10^{4}
	Rear bearing hole	-9.87×10^{4}	-9.65×10^{4}	
II	Front bearing hole	-8.48×10^{4}	-3.346×10^{5}	1.77×10^{5}
	Rear bearing hole	-6.832×10^{4}	-1.15×10^{5}	
III	Front bearing hole	2.72×10^{5}	6.3×10^{4}	-0.98×10^{5}
	Rear bearinghole	3.16×10^{5}	1.57×10^{5}	5.46×10^{5}

Table 3: Mechanical parameters of the improved box body's materials

Components	Materials	E(Mpa)	μ	ρ (kg m^{-3})	σ_s (Mpa)
Upper box body	QT350	1.69e11	0.275	7300	220
Lower box body	QT350	1.69e11	0.275	7300	220
The inner gear ring	17CrNi2Mo	2.00e11	0.3	7870	420
The torque arm	QT400	1.69e11	0.275	7300	250

strength. The attributes of the materials of each component of the improved box body are shown in Table 3.

Meanwhile it is easy to produce stress concentration on the connecting portion of the supports on the two ends of the torque arm and here the transitional connecting mode or fixation mode of the box body can be improved to reduce stress concentration.

MODAL ANALYSIS AND STRUCTURAL IMPR OVEMENT OF GEAR BOX

When performing modal analysis, the box body, gear drive system and input shaft are regarded as a single integral model (Liang *et al*., 2004), as shown in Fig. 3. In the preliminary design, the torque arm is connected to the cabin of the wind turbine generator using high strength bolts and at this time the two ends of the torque arm are supported by fixed supports. Software of Ansys is adopted for modal analysis and the inherent frequency and the mode of vibration of the first 10 stages of the gear box are determined, as shown in Table 4. Fig. 9 shows the natural mode of vibration of the fourth stage at this time.

It can be seen through the analysis results that the inherent frequency and displacement of the gear box at each stage are large, so that its structure is improved: the two ends of the torque arm are supported by elastic constraints rather than fixed constraints, i.e. , a rubber bearing is adopted for supporting the torque arm and the elastic stiffness is 160 KN mm^{-1}, as shown in Fig. 10. Modal analysis is performed again, Table 5 shows the inherent frequency and maximum deformation of the first 10 stages under elastic support and Fig. 11 shows the natural mode of vibration of the fourth stage at this time.

It can be seen from Tables 4 and 5 that, compared with the fixed constraints, the inherent frequency and maximum displacement of the gear box at each stage are significantly reduced by adopting elastic support constraints, thus the elastic constraints can achieve the effects of buffering and damping more efficiently.

FREQUENCY CATCHING ANALYSIS OF GEAR BOX

It can be seen through modal analysis that the inherent frequency of the sixth stage (23.224 HZ) of the

Table 4: Intrinsic mode in fixed support of the gearbox

The stage	Maximum displacement/mm	f/HZ	The stage	Maximum displacement/mm	f/HZ
1	0.50134	24.599	6	3.9837	182.75
2	0.70434	96.691	7	0.4836	186.63
3	0.35565	112.62	8	2.9347	195.47
4	3.3097	159.2	9	0.94556	198.49
5	3.3034	159.77	10	0.76703	218.51

Table 5: Intrinsic mode in elastic support of the gearbox

The stage	Maximum displacement/mm	f/HZ	The stage	Maximum displacement/mm	f/HZ
1	0.10028	0	6	0.19518	23.224
2	0.10028	0	7	1.0456	50.851
3	0.22536	2.3319	8	1.0559	51.193
4	0.24148	2.543	9	1.5282	60.089
5	0.21218	16.998	10	0.39238	70.194

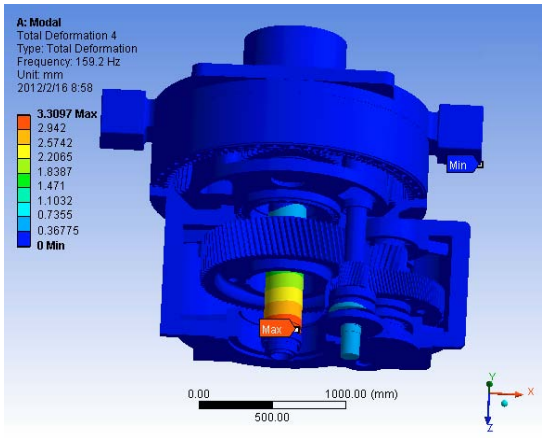

Fig. 9: Gearbox's mode of vibration of fourth stage in fixed support

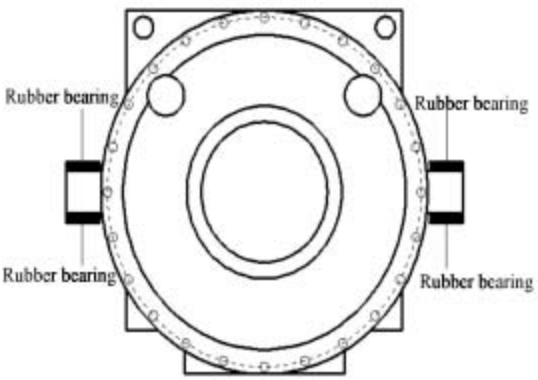

Fig. 10: Elastic supporting mode of the box

gear box draws closer to the gear-mesh frequency (26.5 HZ) of the planetary gear train, where the danger of resonance is present. Software of Matlab is applied to the

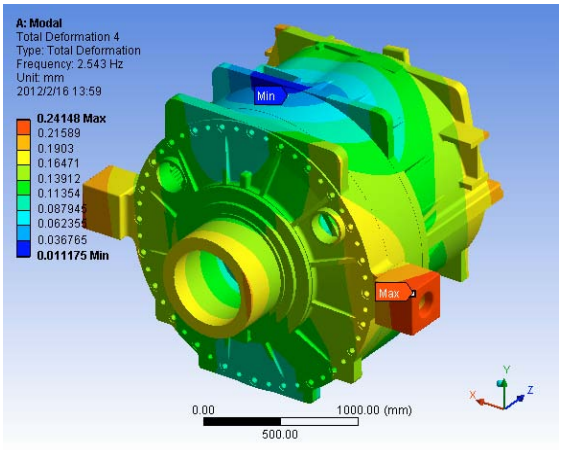

Fig. 11: Gearbox's mode of vibration of fourth stage in elastic support

gear box and planetary gear train to perform frequency catching characteristic analysis (Zhang and Wu, 2011) and the results are shown in Fig. 12. Fig. 12a shows the variation relationship of the speed of the planet carrier as time passes; 12(b) shows the variation relationship of vibratory displacement of the gear box as time passes under motivation of gear-mesh frequency; and 12(c) shows the frequency domain response of the displacement of the gear box.

It can be known through Fig. 12 that the planet carrier can speed up to the rated speed and the gear-mesh frequency of the planetary gear train is not captured by the inherent frequency of the system. The amplitude of the gear box under the motivation of the gear-mesh frequency is very small (the maximum amplitude is less than 1 mm) and the influence to the system can be neglected. Therefore the system is safe because there is no resonance present.

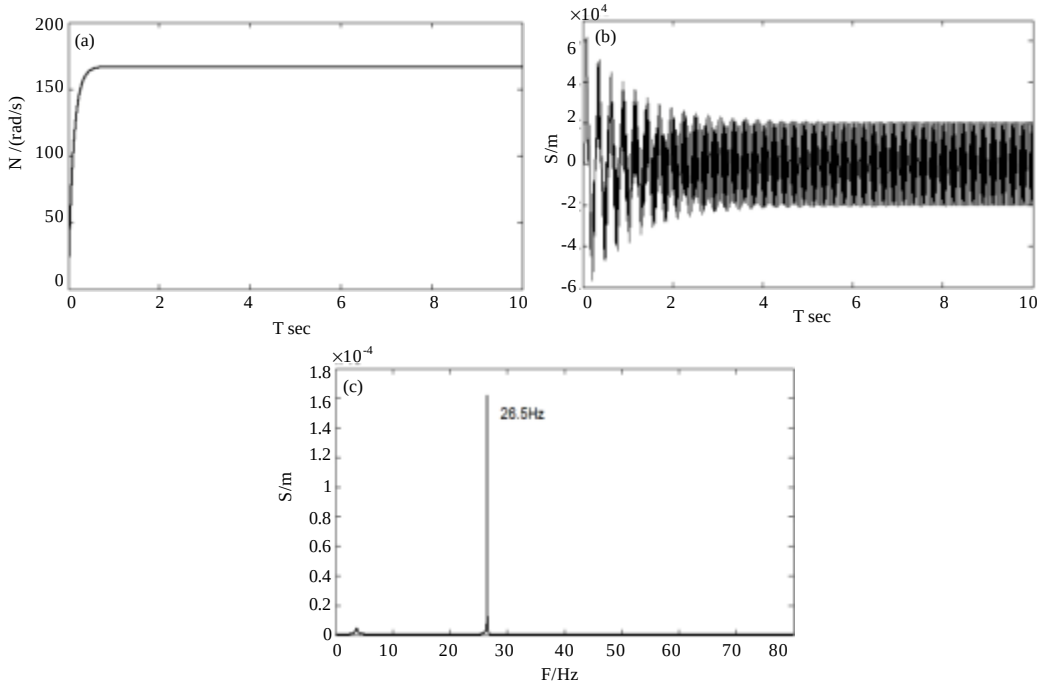

Fig. 12: System's response and spectrum diagram

CONCLUSION

This study provides a new method for analyzing the performance of the heavy structural parts and the dynamic and static characteristics of the heavy structural parts can be described more accurately by integrating statics analysis, modal analysis and frequency catching characteristic analysis.

The static load of each bearing hole of the box body is calculated and static strength is analyzed. Safer materials of the upper and lower box bodies are replaced by materials which meet the strength requirements and have lower costs, thereby lowering costs under the premise of not influencing safety performance, thus the box body is more economic and practical.

The system is supported by elastic constraints instead of fixed constraints and the gear box is conducted integrally with modal analysis to determine the inherent frequency and the type of vibration at each stage and the improved structure reduces vibration and noise.

On the basis of the modal analysis, frequency catching characteristic analysis is performed on components which easily produce resonance and it is proven that the gear-mesh frequency of the planetary gear train will not be captured by the inherent frequency of the system and the system will not undergo the frequency beat phenomenon.

The static strength analysis shows that stresses on the supports on the two ends of the torque arm of the box body are high and distributed more collectively and the transition modes here or the support modes of the box body can be further improved to reduce stress concentration.

Harmonic response analysis and response spectrum analysis can be performed on the basis of system's modal analysis, thereby further analyzing the dynamic performance of the gear box.

Frequency catching analysis is adopted to study the dynamic response characteristics of the large gear boxes; this method is proposed for the first time in this study, thereby providing a novel method for reducing vibration and noise and avoiding resonance in large mechanisms. This study provides a theoretical basis for manufacturing and processing similar large gear boxes, as well as references for designing and checking large vibration systems and has a certain guiding role for researching relative problems. The megawatt gear box designed in the study has been applied in the engineering of 2.0 MW wind power generators of some plants and at present, all gear boxes are functioning well and none have failed or lost their effects.

ACKOWLEDGMENTS

This research is supported by the National Natural Science Foundation of China (51375320), Hi-tech industry

development major key technology project in Si Chuan province (11kjt-04) and Key laboratory open funds authorized by China's ministry of education in Southwest University of Science and Technology (11zxzk04).

REFERENCES

Ge, Z.Q., K.G. Uwe, L.M. Lisa, L. Xie and Z.H. Song, 2010. Fault detection in non-Gaussian vibration systems using dynamic statistical-based approaches. Mech. Syst. Sig. Process., 24: 2972-2984.

Han, Q.K., X.H. Chen, H.L. Yao, W. Sun and B.C. Wen, 2008. Frequency capture simulation and experiment of a rotor system with elastic supports. J. Vib. Shock, 27: 63-66.

Herbert, G.M., S. Iniyan and R. Goic, 2010. Performance, reliability and failure analysis of wind farm in a developing country. Renewable Energy, 35: 2739-2751.

Kusiak, A. and W. Li, 2011. The prediction and diagnosis of wind turbine faults. Renewable Energy, 36: 16-23.

Liang, S.M., W. Luo, J.G. Xu and L.J. Xu, 2004. Modal analysis of swing movable teeth reducer by using finite element method. J. Sichuan Univ. Eng. Sci., 36: 77-80.

Soua, S., L. Cebulski, T.H. Gan and B. Bridge, 2011. Online monitoring of a power slip-ring on the shaft of a wind power generator. Insight, 53: 321-329.

Tian, Z.G., T.D. Jin, B.R. Wu and F.F. Ding, 2011. Condition based maintenance optimization for wind power generation systems under continuous monitoring. Renewable Energy, 36: 1502-1509.

Yao, X.J. and J. Song, 2009. The Principle and Application of the Wind Power Generation. China Machine Press, China, pp: 74-78.

Yi, P.X., L.J. Dong and Y.X. Chen, 2012. The multi-objective optimization of the planet carrier In wind turbine gearbox. Front. Mech. Eng. Mat. Eng., 184-185: 565-569.

Zhang, L.A. and J.Z. Wu, 2011. Frequency capture characteristics in wind blade fatigue loading process. J. Sichuan Univ. Eng. Sci., 43: 248-252.

Zhang, N., X.L. Hou and B.C. Wan, 2009. Characteristics of frequency capture of nonlinear vibration systems. J. Northeastern Univ., 30: 1170-1173.